Letter

Geometry of the vapor layer under a Leidenfrost hydrogel sphere

Vicente L. Diaz-Melian,[1] Isaac C. D. Lenton,[1] Jack Binysh,[2,*] Anton Souslov,[3] and Scott R. Waitukaitis[1,†]

[1]*Institute of Science and Technology Austria, Am Campus 1, 3400 Klosterneuburg, Austria*

[2]*Institute of Physics, University of Amsterdam, Science Park 904, 1098 XH Amsterdam, The Netherlands*

[3]*TCM Group, Cavendish Laboratory, JJ Thomson Avenue, Cambridge CB3 0HE, United Kingdom*

(Received 9 July 2025; accepted 13 March 2026; published 14 May 2026)

A floating Leidenfrost droplet exhibits curvature inversion of its underside, due to the balance of vapor pressure and surface tension. Using interferometric imaging, we find different behavior for a levitated hydrogel sphere. Curvature inversion is observed briefly just after deposition, but quickly gives way to a steady state with no inversion. We show the essential role of vaporization in shaping the underbelly of the hydrogel, where changes due to direct mass loss are more significant than the balance of vapor pressure and elastic forces.

DOI: 10.1103/m7gr-2t6j

A liquid droplet deposited on a hot surface just above its boiling point evaporates quickly and violently. However, at much higher temperatures, an unexpected phenomenon occurs: the droplet levitates and remains floating above the surface for extended periods. This counterintuitive behavior is known as the Leidenfrost effect, and it arises due to the formation of a vapor layer beneath the droplet. This vapor layer insulates the droplet from the surface and simultaneously supports its weight, allowing it to levitate [1–3]. The Leidenfrost effect provides a fundamental framework for understanding fluid–structure interactions, with industrial applications ranging from controllable wetting [4–6] and optimized heat exchange [7–9] to high-temperature spray cooling in metallurgical processes [10,11]. Leidenfrost physics has been extensively studied in simple liquids [12–19] and sublimable solids [20–23], where both experimental [24–31] and theoretical [32–35] efforts have characterized droplet morphology and surface temperature profiles in relation to the droplet's ability to float. More recently, this phenomenon has been extended to vaporizable soft solids, such as hydrogel spheres, which exhibit two distinct types of Leidenfrost behavior [36,37]. At high approach velocities, these spheres make contact with the surface, leading to high-frequency surface oscillations that harvest energy and lead to sustained bouncing [36]. At low velocities, they enter a 'normal' floating state that, in many respects, resembles the classical liquid Leidenfrost state [37].

The morphology beneath Leidenfrost droplets arises from a balance between surface tension, vapor pressure, and gravity. Burton *et al.* investigated this balance experimentally using high-speed interferometric imaging through a transparent, heated substrate [24]. Their results revealed a rim with saddle points and extrema, indicating that the lower facet of the droplet is not flat but exhibits a curvature inversion—i.e., a 'pocket' of vapor exists below the droplet. This shape had been predicted by Snoeijer *et al.*, whose analytical work showed that the curvature inversion becomes more pronounced with increasing droplet radius [32]. For soft vaporizable solids, one might imagine that the shape of the underbelly should reflect a balance between elastic forces and vapor pressure. However, unlike liquid droplets, where material can always flow to achieve energetic balance, solids can only deform (elastically or plastically) and lose material—they have no flow internally. Hence, fundamental differences between the observed shapes in the two cases can be expected.

In this work, we experimentally measure the geometry underneath a Leidenfrost-floating soft solid. We find that the curvature inversion predicted for elastic objects [38] is lost over time due to vaporization-induced shape changes. An initial elastic inversion forms as the hydrogel sphere approaches the hot surface, but rapidly transitions to a steady state without a vapor pocket and with a mostly flat interface. We propose that this transition results from irreversible deformation of the sphere caused by continued vaporization. Using simulations, we qualitatively reproduce our observations. Our results emphasize the central role of vaporization in altering the shape of Leidenfrost-levitated solids, a mechanism that is fundamentally different from that in liquids.

The experimental setup is shown in Fig. 1(a). We use a suction cup to attach a hydrogel sphere (radius $a \approx 7\,\mathrm{mm}$) to a string, which is connected to a weight sensor and a piezo motor. The hot surface below the hydrogel is a wedged sapphire window, chosen for its good heat conduction and transparency. We lower the hydrogel toward the substrate at a constant speed ($\sim 33\,\mu\mathrm{m/s}$) with the piezo motor (Agilis AG-LS25). The window sits on a hot plate, with an aperture that permits an expanded, 633 nm laser (Thorlabs HNL210L) to pass through. This beam reflects off the upper surface of the window and the lower surface of the hydrogel to create an interference pattern, which is recorded by a camera (Phantom

*Present address: Department of Mechanical Engineering, University of Birmingham, B15 2TT Birmingham, United Kingdom.

†Contact author: Scott.Waitukaitis@ist.ac.at

Published by the American Physical Society under the terms of the Creative Commons Attribution 4.0 International license. Further distribution of this work must maintain attribution to the author(s) and the published article's title, journal citation, and DOI.

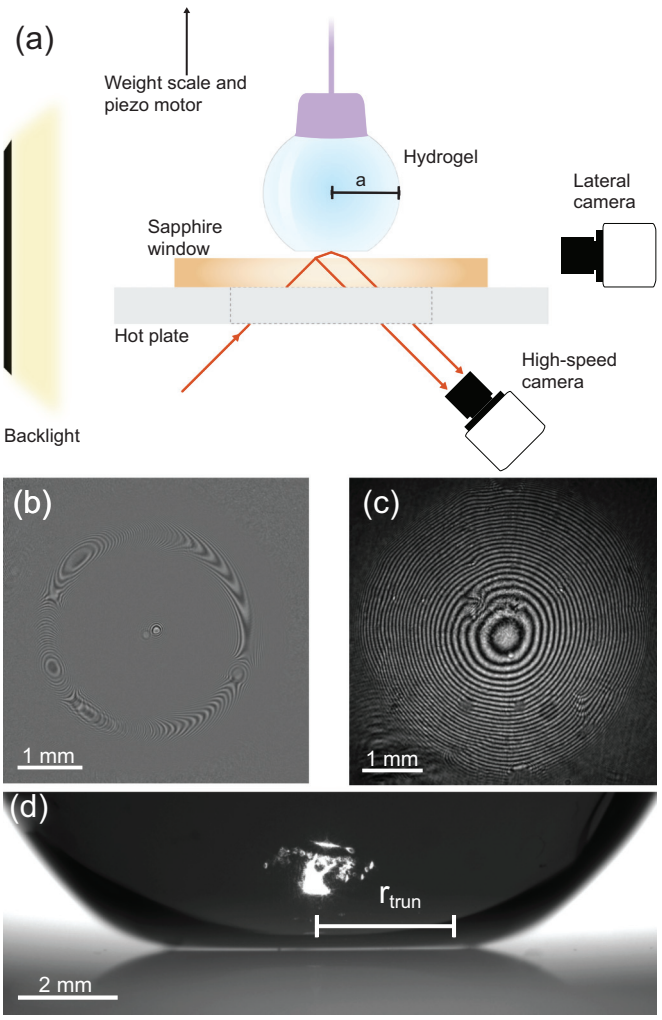


FIG. 1. Experimental setup and key observations. (a) We use a piezo motor to slowly lower a hydrogel sphere connected to a string toward a hot (∼220 °C) sapphire window. A weight sensor at the top of the string allows us to determine how much of the hydrogel is supported by the vapor layer. The hot plate below the sapphire window has an aperture that allows an expanded, 633 nm laser to pass through. A high-speed camera records the interference pattern produced from reflections at the top of the window and the bottom of the hydrogel, while a second camera records from the side. (b) When a water droplet is placed on the window, we observe a steady state with a rim pattern and both saddle/minima features, indicating a curvature inversion beneath the droplet. (c) In contrast, the steady-state pattern for a hydrogel only has concentric rings, indicating the absence of curvature inversion. (d) View of the gap below the hydrogel as seen by the side-view camera, with truncated radius (r_{trun}) indicated.

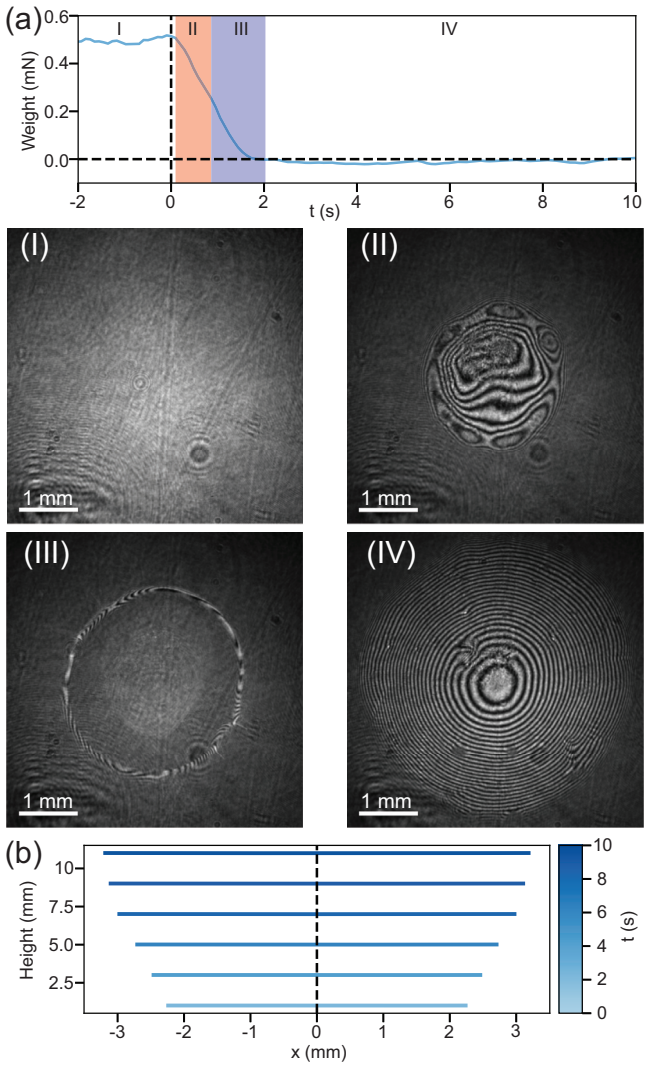


FIG. 2. Time evolution of the interference pattern. (a) Weight of the hydrogel supported by the vapor as a function of time, with key points indicated (I–IV) and corresponding interferometric images. In region I, the weight is carried fully by the string, and no features are present in the interference pattern. At $t = 0$, the hydrogel starts interacting with the vapor (region II), and the interference pattern shows a distinct rim with saddle/minima points, indicating curvature inversion. In region III, the rim destabilizes, and the underside of the hydrogel enters into oscillations. In region IV, the oscillations disappear, resulting in stable floating of the hydrogel and a stable interference pattern without any curvature inversion. (b) Reconstructed height profile of the hydrogel underside in region IV at different times, indicating it is essentially flat. As we show in Supplemental Material, there is a very slight upward curvature [39].

v1612). A second camera (Basler a2A 1920) simultaneously records from the side.

Figure 1(b) first shows the steady-state interference pattern of a liquid droplet. A prominent rim of saddle and extrema points indicates the well-known curvature inversion [24]. In the case of a soft solid, one naturally suspects that the interplay of elasticity and vapor pressure should create a similar inversion, as our recent model has indicated [38]. Our experiments, however, reveal that such reasoning prevails only briefly. As shown in Fig. 1(c), the steady state for a floating hydrogel has no rim of saddles/minima, but rather just an interference pattern of concentric rings, which indicates the absence of curvature inversion. By comparing the radius at which the rings are no longer visible to the 'floating' radius, r_{trun}, of the hydrogel seen from the side-view camera Fig. 1(d), we conclude that the absence of an inversion rim is not due to any limit in the field of view of our interferometric images (see Supplemental Material [39]).

In Fig. 2, we present the time evolution toward this steady state in detail. Panel (a) shows the weight of the hydrogel, supported by the vapor layer as a function of time, with key regimes indicated by Roman numerals (I–IV) and colors. In regime I, the weight is fully supported by the string, indicating that no vapor layer has formed; hence, no interference features are present [Fig. 2(a) image I]. At $t = 0$, the hydrogel just begins interacting with the vapor, and in the red region (II), we observe a curvature-inversion rim (image II). We only observe this inversion very briefly—in the subsequent blue region (III), the rim destabilizes, giving way to rapid (kHz) oscillations that are accompanied by audible whistling. These oscillations are also short lived; after the weight is fully supported by the vapor, the stable regime (IV) is reached, where only concentric rings are present, and there is no inversion. In this regime, the floating radius grows steadily with time, and the number of rings steadily increases (see Supplemental Video 1 [39]). Figure 2(b) shows the reconstructed height profiles in the region IV at different times, as determined by extracting the radial extent of each ring and assigning a height difference of one-half wavelength. Because absent inversion downward curvature is not possible, we conclude that the stable curvature is upward but nearly flat [Fig. 2(b)], however, with height variations on the micrometer scale over millimeter scale that defines the 'floating' radius (see Supplemental Materials [39]).

What gives rise to the observed behaviors? When the hydrogel first approaches the surface, its undeformed shape is spherical, and its initial interaction with the vapor leads to the brief appearance of the anticipated elastic curvature inversion [38]. This is, apparently, unstable, resulting in the oscillations observed in regime III of Fig. 2. We can explain the subsequent flattening through interactions with the hot surface, which cause not only reversible elastic shape changes but also irreversible changes due to vaporization. As soon as the sphere starts vaporizing, it is no longer a sphere, as every parcel of vapor lost permanently alters the shape. Moreover, as elastic forces and vapor pressure conspire to create the initial curvature inversion and oscillations, the edge of the floating region is, on average, closer to the surface than the center, hence it vaporizes faster and disappears.

Once the profile is rather flat, it seems that a second mechanism must kick in that maintains a higher vaporization rate at the edges than at the center to cause the very slight upward curvature. We suspect this is due to the hydrogel cooling the substrate locally, though other factors may contribute [39]. The takeaway is that elastic deformations must also occur throughout; the dominant contribution to the final shape arises from irreversible mass loss due to vaporization.

We lend evidence to these ideas with the experiment sketched in Fig. 3(a). We take a new hydrogel and begin by lowering it toward the hot surface. As soon as its weight is fully carried by the vapor, we stop the piezo motor, which leaves a slight slack in the string. Now we let the sphere float, causing a small vertical slab of thickness δz to be removed due to vaporization. When this exceeds the slack, the string starts carrying the weight, the gap becomes larger, and the vaporization rate is reduced. This leads to an elastic unloading of the sphere and a decoupling from the vaporization-dominant mechanism. When the weight has been fully recovered by

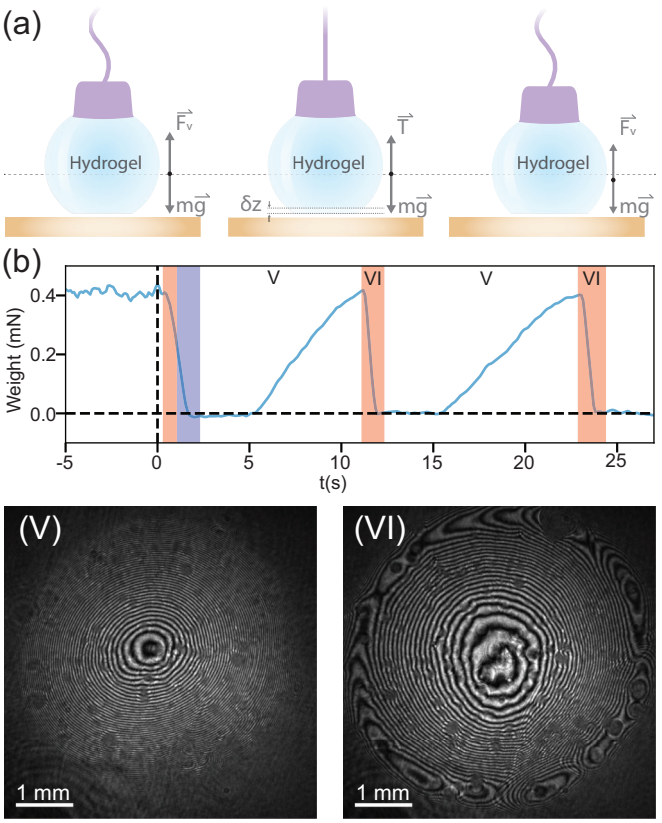


FIG. 3. Temporary recovery of curvature inversion via elastic reloading. (a) To reload the hydrogel elastically, and hence temporarily recover curvature inversion, we start by lowering it just beyond the point where all weight is carried by the vapor, leaving the string slightly loose (left). We then let vaporization occur until a small amount of hydrogel, δz, is removed, resulting in the string again becoming taut (middle). Upon lowering the hydrogel again, the vapor elastically deforms the hydrogel to recover curvature inversion, but only temporarily, as vaporization quickly acts to take it away (right). (b) Weight vs time during multiple iterations of the elastic reloading process. Region V corresponds to the recovery of the weight by the string [middle panel (a)]. Region VI, within the red box, highlights the elastic interplay between the hydrogel and the vapor layer. Once again, evaporation overcomes the curvature inversion, and the hydrogel reaches a stable floating regime without curvature inversion.

the string, we lower the sphere again to reload it elastically and reinitiate the vaporization mechanism, with the prediction that we should (fleetingly) recover the curvature inversion. As shown in Fig. 3(b), this prediction bears true. The upper plot shows the weight carried by the vapor throughout the process, where the transference between the vapor/string for multiple iterations is clearly visible. The images below show the repeatable recovery of the curvature inversion. In V, i.e., after the initial inversion is lost and the sphere has been floating, there are only concentric rings. However, in VI, just after we have elastically reloaded the sphere, the inversion ring reappears—only to quickly be vaporized again. (For the full evolution, see Supplemental Video 2 [39].)

We recover most aspects of the stable regime [IV, Fig. 2(a)] using a simple simulation approach, which involves three steps: (1) using finite element method (FEM) simulations

to calculate the temperature profile of the substrate underneath the hydrogel with average gap height $h_0(t)$ and floating radius $r_{\text{trun}}(t)$; (2) using this temperature profile to numerically calculate the changes in the height profile (and consequently, floating radius) considering the local temperature gradient and a small time interval, δt; and (3) using the known force-balance equation to update the average gap height, h_0, based on the floating radius. In all steps, we take advantage of the fact that the deviations in the height profile (i.e., the slight upward curvature) are much smaller than the average gap height. Details on step 1, i.e., the FEM simulations, can be found in Supplemental Material [39]. Step two is achieved using the mass-loss equation,

$$\delta h(r) = -\frac{\kappa}{\rho L}\frac{T(r) - T_H}{h(r)}\delta t, \tag{1}$$

where κ is the thermal conductivity of the vapor, ρ and L are, respectively, the density and latent heat of the hydrogel, $T(r)$ is the temperature at radius r on the substrate below, and $T_H = 100\,^\circ\text{C}$ is the temperature of the hydrogel. Step three is achieved using the force balance equation for the integrated lubrication pressure *vis-à-vis* the weight of the sphere, given by

$$h_0(t) = \left(\frac{3\pi\eta\kappa\Delta T}{2\rho L}\right)^{\frac{1}{4}} \frac{r_{\text{trun}}(t)}{(mg)^{1/4}}. \tag{2}$$

Here, η is the viscosity of the vapor, ΔT is the (average) temperature difference between the hydrogel and substrate, and mg is the weight of the hydrogel. Though this equation was originally derived for the case of liquid droplets, it was recently shown to be in good agreement for floating hydrogels [37].

Results are shown in Fig. 4 and the corresponding Supplemental Video [39]. Panel (a) shows the (relative) height profiles at different times. Similar to the experiments, the model produces an underbelly hydrogel profile that is *almost* perfectly flat, but with a slight upward curvature (which is comparable to the experimental observations; see [39]). In each iteration of the numerical calculation, the truncated radius is extracted from the resulting height profile; this truncated radius then defines the input conditions for the next iteration. Thus, the truncated radius can be used as a control parameter for the simulations. Figure 4(b) shows that the simulated truncated radius (red points) is in agreement with both the experiments (blue points) and the model prediction (solid black line) [37].

Our results underscore the dominant role of mass loss due to vaporization in shaping the long-term height profile beneath a Leidenfrost-floating elastic solid. In hindsight, this makes perfect sense—liquids can flow, and therefore they will always flow until they reach equilibrium. In the case of liquid Leidenfrost droplets, this is set by balancing pressure in the vapor layer, surface tension, and gravity. Even though a liquid droplet loses mass during vaporization, flow is what allows it to maintain its equilibrium shape. Solids, on the other hand, cannot do this. Although curvature inversion emerges in the early stages of a hydrogel sphere's interaction with a hot surface—and can be briefly reinitiated via elastic reloading—it rapidly disappears as irreversible,

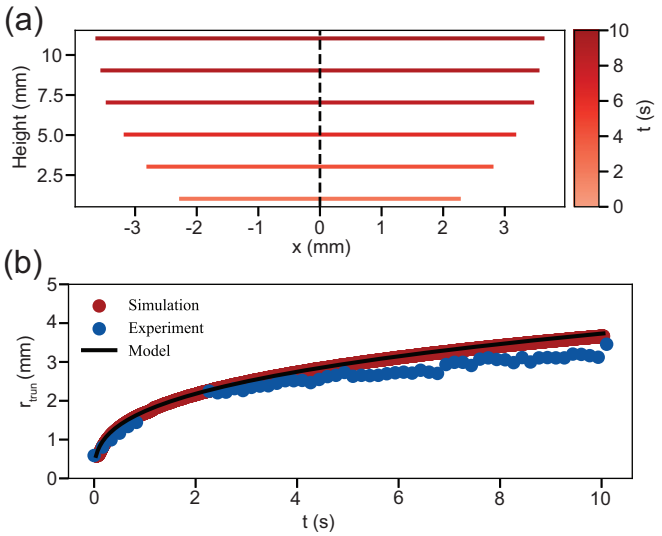


FIG. 4. Simple vaporization model. (a) Height profile underneath the sphere vs time, calculated numerically by iteratively applying Eq. (1) to determine the evolution of the height/radius profile, Eq. (2) to determine the corresponding gap height, and FEM simulations to obtain the updated temperature profile. (b) Truncated radius obtained at each iteration of the numerical calculation, compared with the experimentally measured truncated radius and the model prediction. See Supplemental Material [39] for full simulation details.

vaporization-induced deformations proceed. The solid cannot flow to maintain a minimal energetic state. The simulations show that vaporization is the main mechanism of mass loss and successfully reproduce the key qualitative features of the observed height profile evolution. While our study emphasizes vaporization-driven shape changes, the remnant influence of elasticity remains incompletely explored. A complete analytical treatment of the system—including squeeze flow in the vapor layer, elastic deformations, vaporization dynamics, substrate cooling, and the resulting force balances—is highly complex and beyond what we can assess here. These coupled processes may be more effectively studied using multiphysics simulations to capture all aspects.

This research was supported by the Scientific Service Units of The Institute of Science and Technology Austria (ISTA) through resources provided by the Miba Machine Shop and the Scientific Computing Facility. J.B. acknowledges funding from the European Union's Horizon research and innovation programme under the Marie Sklodowska-Curie Grant Agreement No. 101106500.

V.D. and I.L. contributed to the development of the methodology, formal analysis, and software development. J.B. and A.S. contributed to the conceptualization. V.D. and S.W. contributed to writing and editing the manuscript. S.W. supervised the research activity.

Data availability. The data that support the findings of this article are not publicly available. The data are available from the authors upon reasonable request.

[1] A.-L. Biance, C. Clanet, and D. Quéré, Leidenfrost drops, Phys. Fluids **15**, 1632 (2003).

[2] D. Quéré, Leidenfrost dynamics, Annu. Rev. Fluid Mech. **45**, 197 (2013).

[3] G. Dupeux, M. Le Merrer, C. Clanet, and D. Quéré, Trapping Leidenfrost drops with crenelations, Phys. Rev. Lett. **107**, 114503 (2011).

[4] Y. Wakata, N. Zhu, X. Chen, S. Lyu, D. Lohse, X. Chao, and C. Sun, How roughness and thermal properties of a solid substrate determine the Leidenfrost temperature: Experiments and a model, Phys. Rev. Fluids **8**, L061601 (2023).

[5] M. Jiang, Y. Wang, F. Liu, H. Du, Y. Li, H. Zhang, S. To, S. Wang, C. Pan, J. Yu, D. Quéré, and Z. Wang, Inhibiting the leidenfrost effect above 1,000°C for sustained thermal cooling, Nature (London) **601**, 568 (2022).

[6] M. Shirota, M. A. van Limbeek, C. Sun, A. Prosperetti, and D. Lohse, Dynamic Leidenfrost effect: Relevant time and length scales, Phys. Rev. Lett. **116**, 064501 (2016).

[7] G. G. Wells, R. Ledesma-Aguilar, G. McHale, and K. Sefiane, A sublimation heat engine, Nat. Commun. **6**, 6390 (2015).

[8] T. Tran, H. J. J. Staat, A. Prosperetti, C. Sun, and D. Lohse, Drop impact on superheated surfaces, Phys. Rev. Lett. **108**, 036101 (2012).

[9] A. Grounds, R. Still, and K. Takashina, Enhanced droplet control by transition boiling, Sci. Rep. **2**, 720 (2012).

[10] K. P. Ravikumar, A. Sahoo, and S. S. Mohapatra, Enhancement of spray cooling by modify spray orientation and coolant characteristics, Int. J. Thermofluids **18**, 100342 (2023).

[11] G. Liang and I. Mudawar, Review of spray cooling –Part 1: Single-phase and nucleate boiling regimes, and critical heat flux, Int. J. Heat Mass Transf. **115**, 1174 (2017).

[12] F. Celestini, T. Frisch, and Y. Pomeau, Take off of small Leidenfrost droplets, Phys. Rev. Lett. **109**, 034501 (2012).

[13] A. Bouillant, T. Mouterde, P. Bourrianne, A. Lagarde, C. Clanet, and D. Quéré, Leidenfrost wheels, Nat. Phys. **14**, 1188 (2018).

[14] M. A. J. v. Limbeek, M. H. K. Schaarsberg, B. Sobac, A. Rednikov, C. Sun, P. Colinet, and D. Lohse, Leidenfrost drops cooling surfaces: Theory and interferometric measurement, J. Fluid Mech. **827**, 614 (2017).

[15] G. Graeber, K. Regulagadda, P. Hodel, C. Küttel, D. Landolf, T. M. Schutzius, and D. Poulikakos, Leidenfrost droplet trampolining, Nat. Commun. **12**, 1727 (2021).

[16] P. Chantelot and D. Lohse, Leidenfrost effect as a directed percolation phase transition, Phys. Rev. Lett. **127**, 124502 (2021).

[17] S. Shi, C. Ma, S. Hardt, and C. Lv, Leidenfrost propulsion on symmetric textured surfaces via spontaneous symmetry breaking, Sci. Adv. **11**, eadt6677 (2025).

[18] H. Linke, B. J. Alemán, L. D. Melling, M. J. Taormina, M. J. Francis, C. C. Dow-Hygelund, V. Narayanan, R. P. Taylor, and A. Stout, Self-propelled Leidenfrost droplets, Phys. Rev. Lett. **96**, 154502 (2006).

[19] X. Ma, J.-J. Liétor-Santos, and J. C. Burton, Star-shaped oscillations of Leidenfrost drops, Phys. Rev. Fluids **2**, 031602(R) (2017).

[20] T. R. Cousins, R. E. Goldstein, J. W. Jaworski, and A. I. Pesci, A ratchet trap for Leidenfrost drops, J. Fluid Mech. **696**, 215 (2012).

[21] G. Lagubeau, M. Le Merrer, C. Clanet, and D. Quéré, Leidenfrost on a ratchet, Nat. Phys **7**, 395 (2011).

[22] G. Dupeux, T. Baier, V. Bacot, S. Hardt, C. Clanet, and D. Quéré, Self-propelling uneven Leidenfrost solids, Phys. Fluids **25**, 051704 (2013).

[23] S. Dorbolo, N. Vandewalle, and B. Darbois Texier, Spontaneous rotation of an ice disk while melting on a solid plate, Phys. Fluids **28**, 123601 (2016).

[24] J. C. Burton, A. L. Sharpe, R. C. A. van der Veen, A. Franco, and S. R. Nagel, Geometry of the vapor layer under a Leidenfrost drop, Phys. Rev. Lett. **109**, 074301 (2012).

[25] A. Bouillant, T. Mouterde, P. Bourrianne, C. Clanet, and D. Quéré, Symmetry breaking in Leidenfrost flows, Phys. Rev. Fluids **3**, 100502 (2018).

[26] I. U. Vakarelski, N. A. Patankar, J. O. Marston, D. Y. C. Chan, and S. T. Thoroddsen, Stabilization of Leidenfrost vapour layer by textured superhydrophobic surfaces, Nature (London) **489**, 274 (2012).

[27] S. Hidalgo-Caballero, Y. Escobar-Ortega, and F. Pacheco-Vázquez, Leidenfrost phenomenon on conical surfaces, Phys. Rev. Fluids **1**, 051902(R) (2016).

[28] F. Pacheco-Vázquez, R. Ledesma-Alonso, J. Palacio-Rangel, and F. Moreau, Triple Leidenfrost effect: Preventing coalescence of drops on a hot plate, Phys. Rev. Lett. **127**, 204501 (2021).

[29] A. Bouillant, B. Lafoux, C. Clanet, and D. Quéré, Thermophobic Leidenfrost, Soft Matter **17**, 8805 (2021).

[30] F. Pacheco-Vázquez, M. Aguilar-González, and L. Victoria-García, Designing Leidenfrost puddles, Phys. Rev. Lett. **133**, 234001 (2024).

[31] D. Paulovics, T. Frisch, C. Raufaste, and F. Celestini, Leidenfrost jets, Phys. Rev. Fluids **9**, L112001 (2024).

[32] J. H. Snoeijer, P. Brunet, and J. Eggers, Maximum size of drops levitated by an air cushion, Phys. Rev. E **79**, 036307 (2009).

[33] T. Baier, G. Dupeux, S. Herbert, S. Hardt, and D. Quéré, Propulsion mechanisms for Leidenfrost solids on ratchets, Phys. Rev. E **87**, 021001(R) (2013).

[34] B. Sobac, A. Rednikov, S. Dorbolo, and P. Colinet, Leidenfrost effect: Accurate drop shape modeling and refined scaling laws, Phys. Rev. E **90**, 053011 (2014).

[35] B. Sobac, A. Rednikov, and P. Colinet, Small Leidenfrost droplet dynamics, J. Fluid Mech. **1010**, A47 (2025).

[36] S. R. Waitukaitis, A. Zuiderwijk, A. Souslov, C. Coulais, and M. van Hecke, Coupling the Leidenfrost effect and elastic deformations to power sustained bouncing, Nat. Phys **13**, 1095 (2017).

[37] S. Waitukaitis, K. Harth, and M. van Hecke, From bouncing to floating: The Leidenfrost effect with hydrogel spheres, Phys. Rev. Lett. **121**, 048001 (2018).

[38] J. Binysh, I. Chakraborty, M. V. Chubynsky, V. L. D. Melian, S. R. Waitukaitis, J. E. Sprittles, and A. Souslov, Modeling Leidenfrost levitation of soft elastic solids, Phys. Rev. Lett. **131**, 168201 (2023).

[39] See Supplemental Material at http://link.aps.org/supplemental/10.1103/m7gr-2t6j for supplementary videos, complementary data, and calculations.